Joule

CellPress

Article

Covalent bonding strategy to enable non-volatile organic cation perovskite for highly stable and efficient solar cells

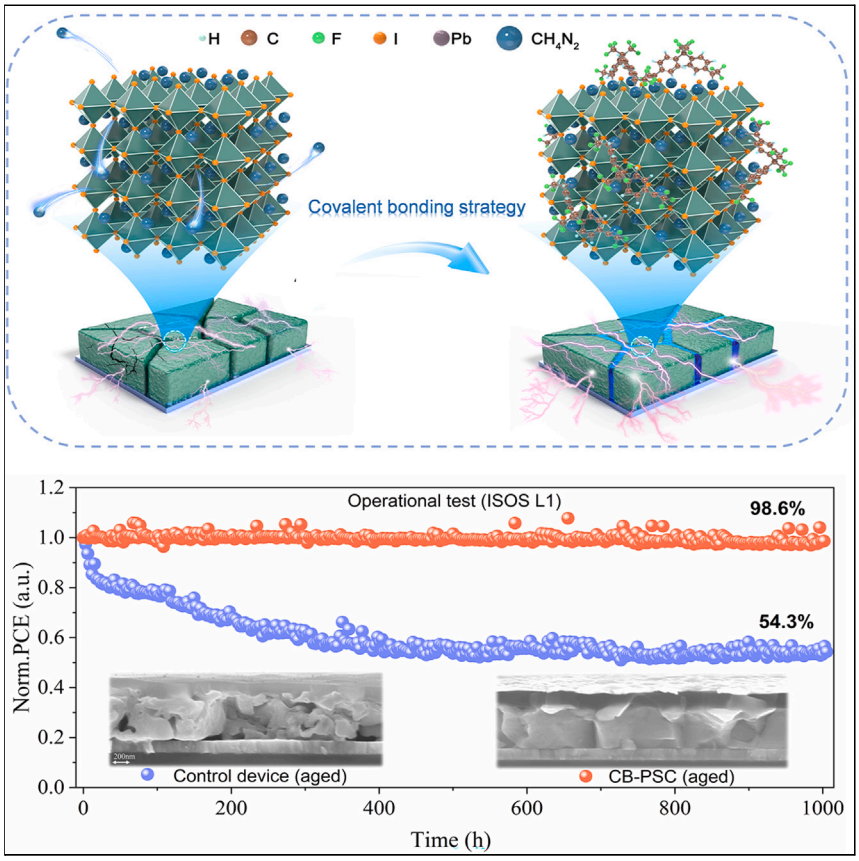

The loss of volatile organic components from perovskites triggers a series of undesirable results, including ion migration, increased defects, and organic vapors, deteriorating the efficiency and stability of perovskite solar cells (PSCs). Here, we introduced bis-diazirine molecules to covalently bond with the organic cations in perovskites, which effectively inhibited the loss of organic components from perovskites during annealing and operation. The resulting optimized PSCs achieved a high certified efficiency of over 24% with long operational stability of over 1,000 h.

Kai Liu, Saqib Rafique, Stefania F. Musolino, ..., Jeremy E. Wulff, Anran Yu, Yiqiang Zhan

wulff@uvic.ca (J.E.W.)
aryu@fudan.edu.cn (A.Y.)
yqzhan@fudan.edu.cn (Y.Z.)

Highlights

Bis-diazirine molecules covalently bond with organic components of perovskites

The process suppressed the formation of vacancies and alleviated ion migration

The generation of metallic Pb under the stress of light and heat is inhibited

The efficient PSC retained 98.6% of the initial efficiency after 1,000 h of operation

Liu et al., Joule 7, 1–18
May 17, 2023
https://doi.org/10.1016/j.joule.2023.03.019

Please cite this article in press as: Liu et al., Covalent bonding strategy to enable non-volatile organic cation perovskite for highly stable and efficient solar cells, Joule (2023), https://doi.org/10.1016/j.joule.2023.03.019

Joule

CellPress

Article

Covalent bonding strategy to enable non-volatile organic cation perovskite for highly stable and efficient solar cells

Kai Liu,[1] Saqib Rafique,[1] Stefania F. Musolino,[2] Zenghua Cai,[3] Fengcai Liu,[1] Xiaoguo Li,[1] Yongbo Yuan,[4] Qinye Bao,[5] Yingguo Yang,[6] Jiao Chu,[7] Xinxin Peng,[4] Cengao Nie,[4] Wei Yuan,[8,9] Sidi Zhang,[9] Jiao Wang,[1] Yiyi Pan,[1] Haijuan Zhang,[1] Xia Cai,[1] Zejiao Shi,[1] Chongyuan Li,[1] Haoliang Wang,[1] Liangliang Deng,[1] Tianxiang Hu,[1] Yaxin Wang,[1] Yanyan Wang,[1] Shiyou Chen,[10] Lei Shi,[7] Paola Ayala,[11] Jeremy E. Wulff,[2,*] Anran Yu,[1,*] and Yiqiang Zhan[1,8,12,*]

SUMMARY

The loss of organic components from perovskites has inevitably triggered a series of undesirable results, including ion migration, increased defects, and organic vapors, which severely limit the performance of perovskite solar cells (PSCs) and impede their progress toward commercial applications. To circumvent this issue, we report a novel covalent bonding strategy by employing bis-diazirine (BD) molecules to covalently bond organic cations of perovskites. Experimental and *ab initio* simulation results confirmed the efficacy of BD molecules to strongly immobilize the organic cations and eventually enhance the thermal, illumination, and electrical bias resistance properties of perovskites. Consequently, highly efficient (24.36% efficiency, certified 24.02%) and ultra-stable PSCs were realized, which retained 98.6% of their initial efficiency even after 1,000 h of operational tests.

INTRODUCTION

Recent years have witnessed remarkable progress in inorganic-organic hybrid perovskite solar cells (PSCs) with power conversion efficiency (PCE) evolving from 3.8% in 2009 to over 25% in 2022 by one-step[1–4] or two-step sequential spin-coating methods.[5] However, given the volatile and migratory nature of organic components in perovskites, the perovskite is prone to degradation under the multiple stimuli of heat, light, and electric fields.[6–9] Thus, realizing the strongly immobilizing organic cations of perovskites for longer operational lifetimes of PCSs remains the key challenge.

Generally, the organic species, especially methylamine ions (MA^+), can easily escape from the grain boundaries of the active layer under working conditions or thermal pressures,[10,11] leading to a series of serious and undesirable consequences. Previous studies[11,12] have shown that under stimuli of heat, trace organic vapors such as MA and formamidine (FA) generated from the perovskite layer can accumulate underneath the gold (Au) electrode, which triggers internal stress to form cracks on the Au surface and simultaneously decays the photovoltaic performance of PSCs. Fan et al.[11] demonstrated that under stimuli of heat and light, the loss of volatile MA^+ could result in the local decomposition of perovskites associated with the release of I_2 vapor. Subsequently, the loss of MA, FA, and I leads to numerous organic cation

CONTEXT & SCALE

Inorganic-organic hybrid perovskite solar cells (PSCs) have attracted great attention due to their excellent optoelectronic properties. However, the volatile organic components in perovskites tend to migrate or even escape from the perovskite layer under the stimuli of heat and illumination, causing numerous vacancies, severe non-radiative recombination, and ion migration in PSCs. Moreover, organic vapors generated from the perovskite layer can accumulate underneath the gold (Au) electrode, which triggers internal stress to form cracks on the Au surface and simultaneously decays the performance of PSCs. Here, we proposed a novel strategy to achieve efficient and stable PSCs through introducing bis-diazirine molecules to immobilize the organic cations by covalent bonds. The resulting PSCs exhibited a high certified efficiency of over 24% with long operational stability of over 1,000 h. We believe that this strategy also possesses great potential in other perovskite-based optoelectronic devices.

Please cite this article in press as: Liu et al., Covalent bonding strategy to enable non-volatile organic cation perovskite for highly stable and efficient solar cells, Joule (2023), https://doi.org/10.1016/j.joule.2023.03.019

and halide ion vacancies at the surface of the perovskite.[13,14] Hui et al.[15] demonstrated that the presence of organic cation vacancies facilitates the migration of iodide ions due to the reduced steric hindrance. In addition, Chen et al.[16] recently observed that I^- can diffuse into organic cation vacancies originated from the initial loss of organic cations. Similarly, Yang et al.[17] demonstrated that mobile I anions tend to fill the vacancies of organic cations as I anti-site substitutions, inducing the deep-level traps in perovskite. More importantly, these studies indicate that iodide migration or diffusion into organic cation vacancies inevitably triggers more iodide vacancies. Unfortunately, these generated vacancies induced by the loss of organic components ultimately affect the photovoltaic performance and stability of PSCs. Moreover, vacancies can also provide the channels for accelerating the ionic migration.[18] In addition, iodide vacancies can easily induce the unsaturated Pb that has been reported as the main factor leading to the generation of metallic lead.[19–24] Last, but not least, the sustained loss of organic species results in non-stoichiometry of perovskites and reconstruction of crystals.[9] Ion migration,[6,18,25,26] metallic Pb,[27,28] and organic vapors[11,12] not only limit the efficiency of PSCs but also induce the degradation of perovskite, thus, severely impacting the long-term operational and thermal stabilities of PSCs. To suppress the loss of organic cations and confine the ion migration at the grain boundaries of perovskites for enhancing the lifespan of devices, several effective approaches including hydrogen bonding[9,29] and conventional crosslinking strategies[30,31] have been proposed. Nevertheless, these approaches are not capable of confining the loss of organic components in the perovskite. For instance, the hydrogen bonding between these molecules and organic cations is generally too weak to shelter the perovskite material when it is exposed to a hostile environment.[32] Similarly, the conventional crosslinking strategy lacks direct and strong bonding with organic cations. Hence, a dense crosslinked polymer network is required to prevent the escape of organic cations to the air, which inevitably impedes the transport of carriers.[31] Thus, it is essential to propose a comprehensive approach capable of strongly bonding organic components of perovskites to reduce the performance losses.

Herein, this work reports a novel covalent bonding strategy by employing bis-diazirine (BD) molecules covalently bonded with organic cations to prevent the loss of organic components of perovskites. In this strategy, the BD molecules decompose into carbenes under mild conditions, enabling them to undergo covalent bonding with organic cations at the grain boundaries.[33] The results showed that the covalent bonding strategy facilitates the ions' immobilization, inhibits the escape of organic components, and eliminates the metallic Pb. Hence, it reveals enhanced thermal, illumination-resisting, and electrical bias-resisting properties of perovskites. Moreover, the hysteresis of devices was greatly reduced by the covalent bonding strategy. The resultant PSCs fabricated by covalent bonding strategy and abbreviated CB-PSCs hereafter achieved an impressive efficiency of 24.36% (band gap 1.53 eV, certified 24.02%) and 23.95% (band gap 1.57 eV), with a remarkably high open circuit voltage of over 1.2 V and excellent operational and thermal stabilities. The CB-PSCs without encapsulation maintained nearly 98.6% of the initial efficiency after continuous operations under 1 sun illumination for 1,000 h at 36°C $\pm$ 3°C and retained 97.6% of the initial efficiency under constant heat at 60°C for almost 590 h, respectively. In comparison, the control device exhibited a 35% loss in the initial PCE only after 200 h. Moreover, it also showed poor thermal stability and reduced to 73% of the initial values after 590 h under constant heat at 60°C. Hence, the improved efficiency and stability of CB-PSCs are attributed to the successful immobilization of organic components by covalent bonding strategies.

[1]Center for Micro Nano Systems, School of Information Science and Technology (SIST), Fudan University, Shanghai 200433, China

[2]Department of Chemistry, University of Victoria, Victoria, BC V8W 3V6, Canada

[3]Jiangsu Key Laboratory of Micro and Nano Heat Fluid Flow Technology and Energy Application, School of Physical Science and Technology, Suzhou University of Science and Technology, Suzhou 215009, China

[4]Hunan Key Laboratory of Super Microstructure and Ultrafast Process, School of Physics and Electronics, Central South University, Changsha, Hunan 410083, China

[5]School of Physics and Electronic Science, East China Normal University, Shanghai 200241, China

[6]Shanghai Synchrotron Radiation Facility (SSRF), Zhangjiang Lab, Shanghai Advanced Research Institute, Chinese Academy of Sciences, 239 Zhangheng Road, Shanghai 201204, China

[7]State Key Laboratory of Surface Physics, Key Laboratory of Micro- and Nano-Photonic Structures (Ministry of Education) and Department of Physics, Fudan University, Shanghai 200433, China

[8]The State Key Laboratory of Photovoltaic Science and Technology, Institute of Optoelectronics, Fudan University, 2005 Songhu Road, Shanghai 200438, China

[9]Department of Chemistry & The State Key Laboratory of Molecular Engineering of Polymers, Fudan University, 2005 Songhu Road, Shanghai 200438, China

[10]Key Laboratory of Computational Physical Sciences (MOE), and State Key Laboratory of ASIC and System, School of Microelectronics, Fudan University, Shanghai 200433, China

[11]Faculty of Physics, University of Vienna, 1090 Vienna, Austria

[12]Lead contact

*Correspondence: wulff@uvic.ca (J.E.W.), aryu@fudan.edu.cn (A.Y.), yqzhan@fudan.edu.cn (Y.Z.)

https://doi.org/10.1016/j.joule.2023.03.019

Please cite this article in press as: Liu et al., Covalent bonding strategy to enable non-volatile organic cation perovskite for highly stable and efficient solar cells, Joule (2023), https://doi.org/10.1016/j.joule.2023.03.019

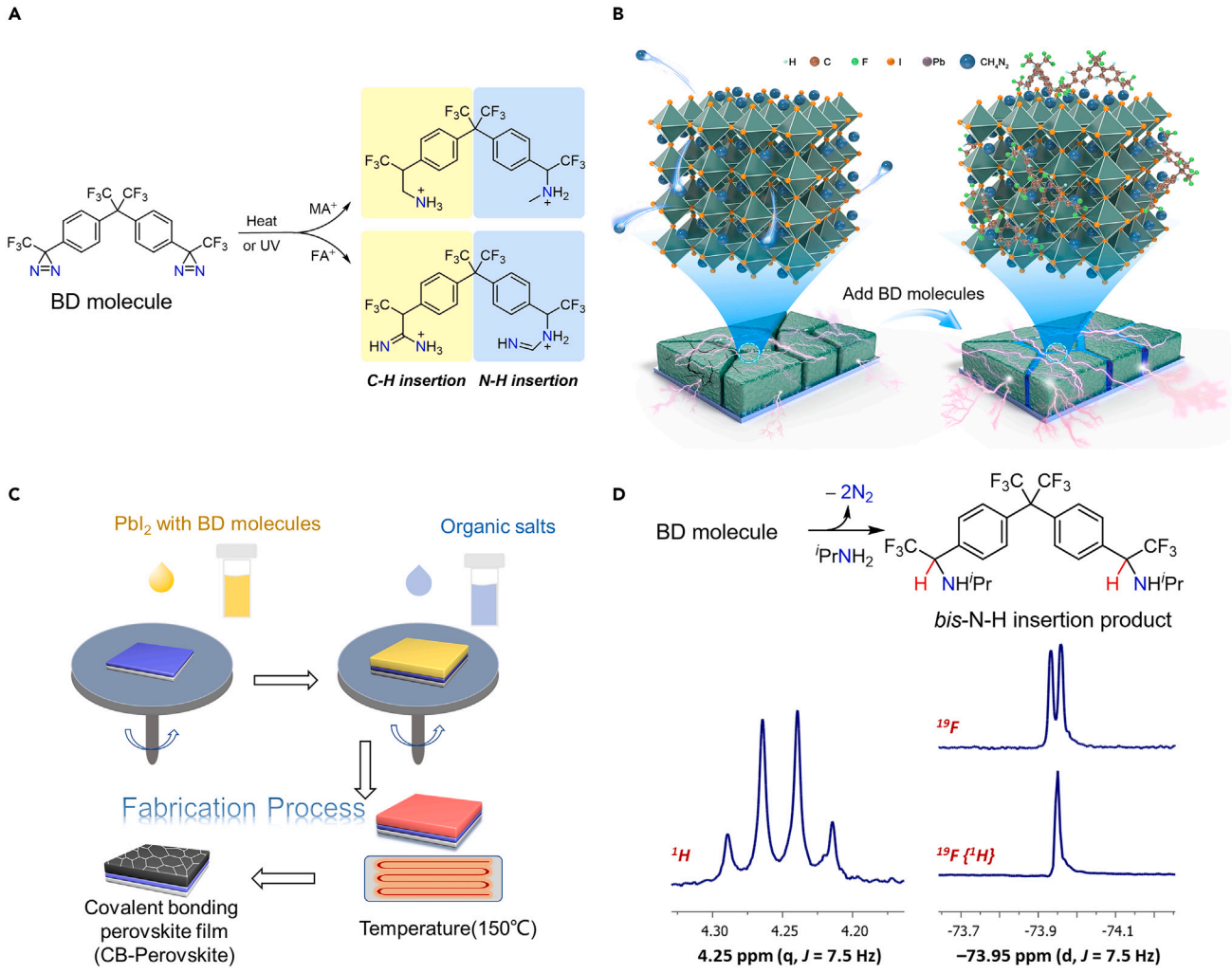

Figure 1. The covalent bonding strategy to realize ultra-stable perovskites

(A) The chemical structure of 3,3′-((perfluoropropane-2,2-diyl) *bis*(4,1-phenylene)) *bis*(3-(trifluoromethyl)-3*H*-diazirine) (BD molecule); expected insertion products between BD molecules and the organic component of perovskites under mild conditions.

(B) Schematic illustrations of the covalent bonding strategy.

(C) Schematic illustration of the perovskite film deposited by the two-step sequential spin-coating method.

(D) bis-N–H insertion product using isopropylamine as a model compound for MA^+. Excerpt of the ^{1}H-NMR spectrum showing the coupling pattern for the proton in the newly formed bond and proton-coupled and proton-decoupled ^{19}F-NMR spectra of the α-CF_3 group.

RESULTS AND DISCUSSION

Covalent bonding strategy

The chemical formula of the BD molecule is shown in Figure 1A. It has been previously demonstrated that this small molecule can crosslink any aliphatic organic molecules containing C–H bonds (or O–H or N–H bonds) through the use of high temperatures or UV light to activate the diazirine groups.[33] Considering the potent crosslinking properties of BD molecules, it is envisioned that by incorporating BD molecules into perovskite, they are likely to bind with organic components by forming covalent bonds, as shown in Figure 1B. Because organic cations are fixed in the perovskite crystal at a certain distance, the lattice matching between the binding sites of BD molecules and organic cations should be investigated first. Figure S1 depicts that the distance of binding sites of BD molecules (9.20 Å) is matching well with the lattice size of FA perovskite (9.01 Å). Moreover,

Please cite this article in press as: Liu et al., Covalent bonding strategy to enable non-volatile organic cation perovskite for highly stable and efficient solar cells, Joule (2023), https://doi.org/10.1016/j.joule.2023.03.019

as depicted in Figure 1C, high-temperature annealing can provide the energy to activate the covalent bonding process. These results are prerequisites for our covalent bonding strategy. Predicted insertion products can form via C–H or, more likely, N–H insertion (Figure 1A). We first employed high-angle annular dark-field (HAADF) and energy dispersive spectroscopy (EDS) to investigate the distribution of BD molecules in perovskites. Figure S2A is a HAADF image of the perovskite, and Figures S2B and S2C are the EDS images of Pb and F. From scanning transmission electron microscopy energy dispersive X-ray spectroscopy (STEM-EDS) mapping of Pb and F, we inferred that these two elements exhibit similar distributions, which also indicates that BD molecules are evenly distributed on the perovskite grains.

To explore the covalent bond formation between BD molecule and MA^+, we carried out separate experiments in solution using isopropylamine as a practical alkyl amine model for MA. Experiments were conducted using solutions of either BD molecule (Figures S3–S9; Notes S1 and S2) or mono-diazirine (MD molecules) analog (trifluoromethyl phenyl diazirine; Figures S10–S13; Note S3) in isopropylamine and MA^+ (Figure S14; Note S4). We observed from the analysis of crude ^{19}F nuclear magnetic resonance (NMR) spectra the efficient formation of N–H and possible C–H insertion products (Figure S9). Isolation and characterization of bis-N–H and mono-N–H products confirmed the efficiency of covalent bond formation between the two molecules (see supplemental information for complete spectral details). In particular, as shown in Figure 1D, the newly formed C–H bond can be observed in the ^1H-NMR spectrum at 4.25 parts per million (ppm), with the presence of a quartet-coupling pattern indicating the presence of a hydrogen coupling with the α-CF_3 group ($^3JH\text{-}F = 7.5$ Hz). This is further confirmed in the ^1H-coupled ^{19}F-NMR spectrum with the appearance of a doublet at -73.9 ppm ($^3JH\text{-}F = 7.5$ Hz) corresponding to the CF_3 group adjacent to the insertion site and in the ^1H-decoupled ^{19}F ($^{19}F(^1H)$)-NMR spectrum with the appearance of the same peak as a singlet. Similar experiments were performed on the solid MA^+ substrate, as shown in Figure S14, a peak of -74 ppm which could be the possible N–H insertion product. Previous publications have demonstrated that MD molecule insertion results are comparable with those from the BD molecules.[34,35] In addition, the MD molecule is an excellent model substrate to help with NMR studies. Therefore, we further used the model substrate to be able to identify insertion products of formamidium iodide (FAI) during the curing step, avoiding the competing oligomerization reaction happening with the BD substrates. Figures S15 and S16 and Note S5 illustrate the NMR spectra resulting from the reaction of the MD with FAI, revealing signals characteristic of insertion products.[36] Furthermore, Fourier transform infrared spectroscopy (FTIR) was employed to prove the existence of the covalent bonds in perovskites. The FTIR results in Figures S17 and S18 and Note S6 also indicate that the BD molecules covalently bonded with perovskites.

The unique role of the covalent bonding strategy in perovskites was further elucidated using first-principles calculations. After subsequent atomic relaxation, the BD molecules were found to stably sustain on the surface of $FAPbI_3$ (Figure 2A). Since BD molecules can connect with both C and N atoms in FA, two insertion types were included in our study (see supplemental information for complete spectral details, Figures S19 and S20, and Note S7). As we can see in Figure 2B, both C–H insertion and N–H insertion types can stably exist. In addition, the related total energy (E_S) of the C insertion type is -5.00 eV/atom, which is similar to -4.99 eV/atom of the N–H insertion. This further demonstrated that both insertion types can stably exist in perovskites, and they are also consistent with FTIR and NMR results.

Please cite this article in press as: Liu et al., Covalent bonding strategy to enable non-volatile organic cation perovskite for highly stable and efficient solar cells, Joule (2023), https://doi.org/10.1016/j.joule.2023.03.019

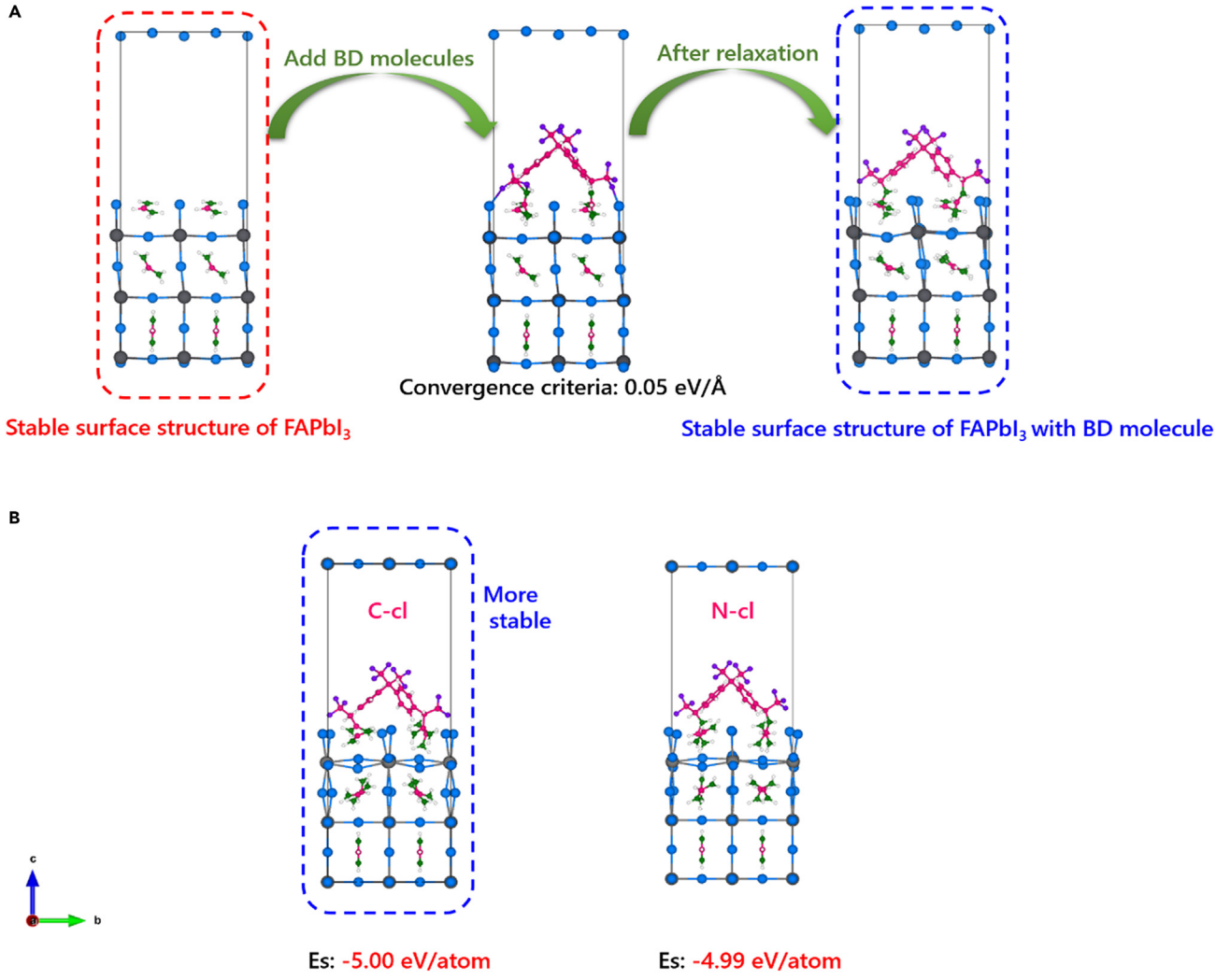

Figure 2. Theoretical simulation of FA perovskites with BD molecules

(A) The process of constructing the stable surface structure of $FAPbI_3$ with BD molecules.

(B) The final surface structures and the related total energy (E_S) of $FAPbI_3$ with BD molecules adsorbed with C and N on FA groups, respectively.

X-ray photoelectron spectroscopy (XPS) analysis was conducted to elucidate the possible hydrogen bond interactions of fluorine atoms with the organic cations[37,38] and to investigate the effect and contribution of fluorine. Since the formation of hydrogen bonds can significantly affect the binding energy of elements, as shown in Figure S21, the XPS spectrum of the N 1s orbital peak showed a negligible deviation after introducing the BD molecules, which indicates that there is no interaction between fluorine groups and perovskites.[37] In addition, after incorporating BD molecules, the XPS spectra of the C 1s orbital peak showed a significant deviation. This is probably due to the interaction between BD molecules and organic cations or the influence of the C element introduced by BD molecules.

All these results confirm the formation of a covalent linkage between BD molecules and organic components of perovskites. Obviously, the CB-perovskite films exhibit strong covalent bonding having a greater binding energy compared with the hydrogen bond. Hence, it enables strongly immobilized organic components.

Please cite this article in press as: Liu et al., Covalent bonding strategy to enable non-volatile organic cation perovskite for highly stable and efficient solar cells, Joule (2023), https://doi.org/10.1016/j.joule.2023.03.019

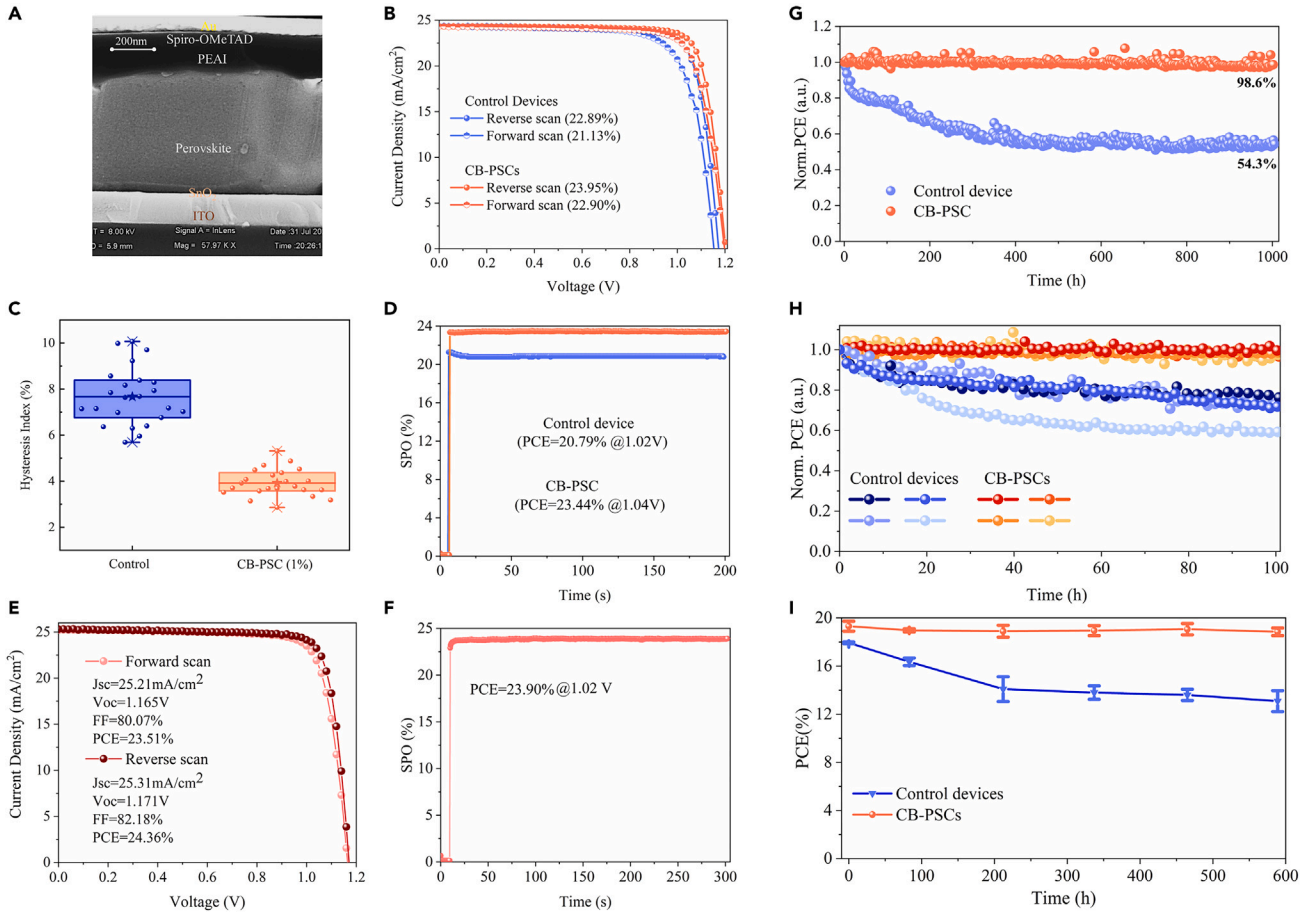

Figure 3. Photovoltaic performance and stability of devices

(A) The cross-sectional SEM image.

(B) Forward scan and reverse scan efficiencies of the champion control device and CB-PSCs (1.3 M FA-based PSC, band gap 1.57 eV).

(C) Hysteresis index of control ad CB-PSCs. HI = $(PCE_{(reverse)} - PCE_{(forward)})/PCE_{(reverse)}$.

(D) Stable power out (SPO) of the control device and CB-PSC (1.3 M FA-based PSC, band gap 1.57 eV).

(E) Forward scan and reverse scan efficiencies of thicker CB-PSC (1.5 M FA-based PSC, band gap 1.53 eV).

(F) Stable power out (SPO) of thicker CB-PSC (1.5 M FA-based PSC, band gap 1.53 eV).

(G) Operational stability of 1.3 M FA-based PSCs under 1,000 h of continuous illumination at 1 sun and under an N_2 atmosphere using white LEDs and MPPT (the initial average efficiencies of control devices and CB-PSCs are 21.51% and 22.45%, respectively).

(H) Operational stability of multiple devices (1.3 M FA-based PSCs) (the initial average efficiencies of control devices and CB-PSCs are 21.02% and 22.67%, respectively).

(I) Stability of devices at 60°C in the N_2 glove box (the initial average efficiencies of control devices and CB-PSCs are 17.93% and 19.31%, respectively).

Photovoltaic performance and stability

An ITO/SnO_2/perovskite (1.3 M FA-based)/ phenethylammonium iodide (PEAI) /spiro-OMeTAD/Au device configuration has been employed (Figure 3A). The concentration of the incorporated BD molecules has been carefully optimized, and the corresponding photovoltaic performance of the CB-PSCs compared with control PSCs has been presented in Figures 3B, S22, and S23, respectively. Owing to the covalent bonding strategy, the efficiency of CB-PSC (1% BD molecules) is enhanced to 23.95% with a V_{oc} of 1.202 V, FF of 81.83%, and J_{sc} of 24.34 mA/cm^2. In addition, the external quantum efficiency (EQE) plots shown in Figure S24 illustrate that integrated J_{sc} obtained from EQE matches well with that extracted from J-V curves (deviations are 3.70% and 3.73% for the control device and CB-PSC, respectively). The corresponding PV parameters (Figure 3B) are summarized in Table S1. The

Please cite this article in press as: Liu et al., Covalent bonding strategy to enable non-volatile organic cation perovskite for highly stable and efficient solar cells, Joule (2023), https://doi.org/10.1016/j.joule.2023.03.019

enhanced V_{oc} and FF are probably ascribed to fewer defects (i.e., organic cations and halide ions vacancies) due to the covalent bonding strategy. In addition, CB-PSC was held at a bias of 1.04 V for nearly 200 s, leading to a higher and more stable power output (SPO) compared with the control device (Figure 3D). The more stable SPO at the maximum point in the timescale of seconds is mainly due to the reduced ion migration in perovskites.[39] To demonstrate the universality of the covalent bonding strategy, we then employed BD molecules in thicker perovskite absorbers on 1.5 M FA-based perovskite (1.53 eV) precursor solution. As a result, a champion PCE of 24.36% (Figure 3E) with a stable SPO of 23.9% (Figure 3F) was achieved with negligible hysteresis. Moreover, the EQE plot of 1.5 M CB-PSCs was shown in Figures S25 and S26 and Note S8, which is also consistent well with J-V curves (deviation is 3.16%). To verify the efficiency of target devices, one of the champion devices was validated by an independent solar cell-accredited laboratory (SIMIT, Shanghai, China) for certification, in which a PCE of 24.02% was measured, as shown in Figure S27.

In addition, as depicted in Figures 3B, 3C, and S23, the covalent bonding strategy enabled less hysteresis compared with the control devices. Usually, ion migration is considered the main factor to trigger the large hysteresis in PSCs.[40] As mentioned above, the initial loss of organic species at grain boundaries and interfaces not only reduces steric hindrance for the migration of halide ions[15] but also induces more halide ions and organic cation vacancies in perovskite.[11,13,16,17] These vacancies also contribute to ion migration.[9,18] Thus, the decreased hysteresis in CB-PSCs is probably attributed to the successful confinement of organic ions by the covalent bonding strategy. Furthermore, this is also in agreement with the more SPO of CB-PSCs (Figure 3D).

Given the fact that ion migration not only causes the hysteresis effect in devices but also plays a critical role in the long-term stability of PSCs,[25,26] we therefore evaluated the effect of covalent bonding strategy on the operational stability of PSCs. Moreover, international organization for standardization (ISOS) testing protocols (ISOS-L-1) for PSCs have been followed.[41] Devices were tested under 1 sun continuous illumination for over 1,000 h in an inert atmosphere. The results (CB-PSC with 1% BD molecules) have shown remarkable operational stability by retaining 98.6% of the initial efficiency even after 1,000 h maximum power point tracking (MPPT) and continuous illumination as shown in Figure 3G, whereas, the control devices decayed to 65% of their initial PCE only after 200 h of the aging test, which is similar to other reports.[12,37] Notably, the control devices exhibited a rapid burn-in loss during the initial period, although this phenomenon was not observed in CB-PSCs. In general, the burn-in loss that occurs in PSCs is probably due to the migration of A-site cations and halide ions.[39,42] Moreover, to avoid any systematic error, the operational stability of multiple PSCs has been studied for shorter durations (100 h). Figure 3H demonstrated that a similar trend has been followed for multiple devices, and the CB-PSCs showed significantly better stability compared with control devices where the initial burn-in losses have been observed. Similarly, after employing the covalent bonding strategy, the operational stability of 1.5 M FA-based PSC has been greatly enhanced (Figure S28). Hence, CB-PSCs proved to be highly stable and efficient compared with their control counterparts. Moreover, the stability and efficiency of our device have outperformed almost all the previously reported works that have used conventional strategies that we have mentioned above (Table S2) and other excellent works published in highly prestigious journals in the recent 2 years (Table S3). Moreover, to improve the integrity and effectiveness of this work and allow for a better extension of the crosslinking

Please cite this article in press as: Liu et al., Covalent bonding strategy to enable non-volatile organic cation perovskite for highly stable and efficient solar cells, Joule (2023), https://doi.org/10.1016/j.joule.2023.03.019

strategy in PSCs, we also investigated the influence of MD on the performance of PSCs. The relevant results are shown in Figures S29 and S30, which illustrate that MD molecules can effectively enhance the performance of PSCs compared with the control devices; however, BD molecules outperformed the MD.

Owing to the fact that the loss of organic components can also be easily triggered by heat and lead to the degradation of perovskites,[9] a thermal stability test (60°C in N_2 glove box) was conducted to investigate the efficacy of the covalent bonding strategy in PSCs during the thermal stress (Figure 3I). The CB-PSCs demonstrated excellent thermal stability and maintained 97.6% of the initial PCE, whereas the control devices retained only 73% of the initial PCE after ~590 h. Similarly, CB-PSCs also exhibited better thermal stability than control devices at 85°C (Figure S31), which further verified the effect of the covalent bonding strategy. In addition, the covalent bonding strategy proved to be equally effective even if the annealing time window has been extended, which is highly desired for large-scale productions such as blade coating. The results for extended annealing time have been presented in Figure S32 and Note S9.

Mechanisms of enhanced photovoltaic performance and stability due to covalent bonding strategy

To further elucidate the enhanced photovoltaic performance and stability caused by the CB-PSCs, the influence of covalent bonding strategy on morphology and crystallization of perovskite films has been studied using X-ray diffraction (XRD), scanning electron microscope (SEM), and grazing incidence wide-angle X-ray scattering (GIWAXS). The XRD spectrum of the control film is consistent with a previously reported work where the perovskite films were fabricated by the sequential spin-coating method.[43–46] The XRD spectrum of the CB-perovskite film (Figure 4A) showed stronger (001) crystal planes of perovskites. The result clearly indicates the enhanced crystallinity of perovskites caused by the inclusion of BD molecules. The enhanced crystallinity of the CB-perovskite film leads to fewer defects of films, which contribute to the higher FF and V_{oc} of CB-PSCs.[44,47] In addition, the CB-perovskite film exhibited a weaker diffracted intensity of lead iodide (PbI_2) than the control film, which is attributed to the effective inhibition of the organic component loss during the annealing process by our strategy.[48] To further confirm the critical role of the covalent bonding strategy in suppressing the loss of organic components, we carried out XRD measurements on films that were subjected to an extended annealing time of 35 min (over-heated film). The results in Figure 4A illustrated that the control film showed a lower intensity of perovskites along with an enhanced intensity of PbI_2. In addition, the CB-perovskite film exhibited better crystallinity of perovskites with slightly increased intensities of PbI_2 after extended heating. These results further demonstrated the effective immobilization of organic components by the covalent bonding strategy. In general, high temperatures provide the energy for crystal growth; however, it also induces the loss of organic components. Thus, there is a trade-off between suppressing the loss of organic components and enhancing the crystallinity of perovskites during annealing. Hence, the better crystallinity of CB-perovskites is probably due to the good prevention of organic component loss during over-heated (35 min, contrary to 15 min) times. This is consistent with the broadened annealing time window depicted in Figure S32. In addition, a low-intensity peak emerged in the CB-perovskite film at 13.2°. Its brief description is presented in Figure S33 and Note S10. Moreover, after incorporating BD molecules, the peak of the perovskite shifts to a smaller angle (Figure S34), which indicates that there is a slight stress in perovskites, which is due to the strong interaction between BD molecules and perovskites. This also indicates the successful reaction between BD molecules

Please cite this article in press as: Liu et al., Covalent bonding strategy to enable non-volatile organic cation perovskite for highly stable and efficient solar cells, Joule (2023), https://doi.org/10.1016/j.joule.2023.03.019

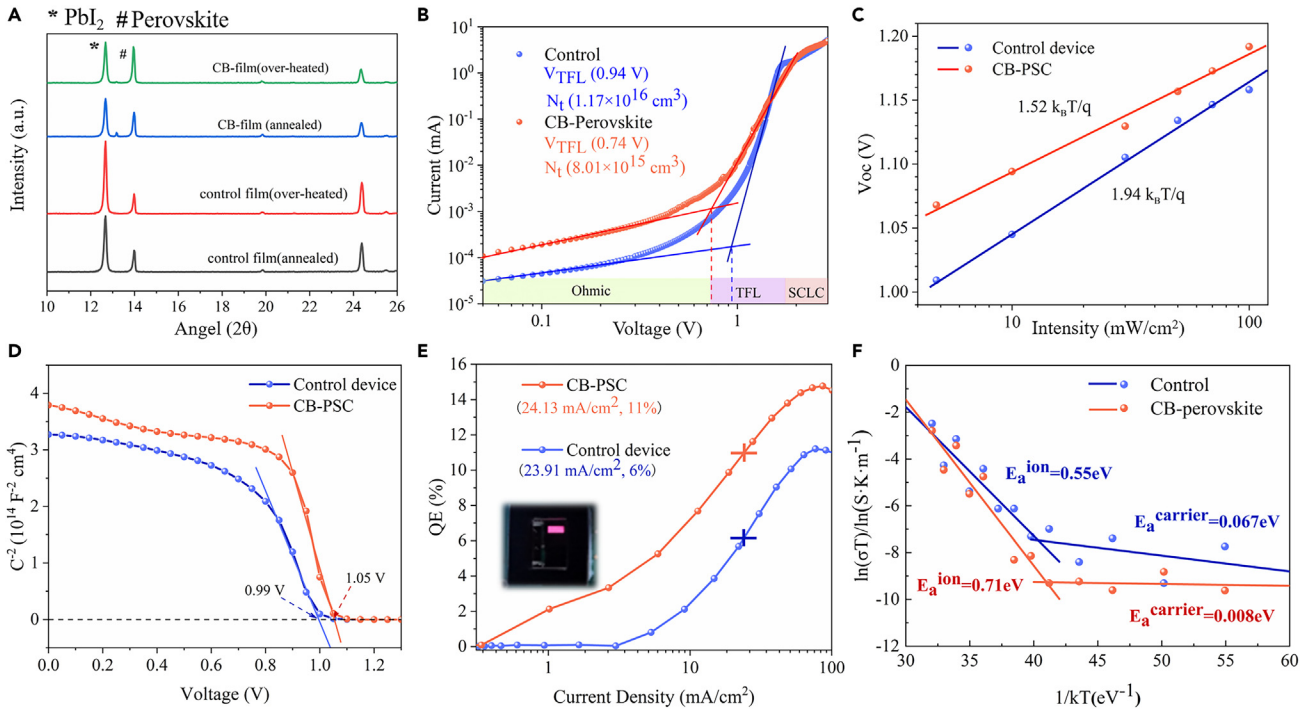

Figure 4. Characterization of perovskite films and devices

(A) XRD peak intensities of PbI_2 and perovskite under different annealing times. "Over-heated": continuous annealing for 20 min at 150°C of pre-annealed perovskite (15 min at 150°C).

(B) SCLC curves of control devices and CB-perovskite electron-only devices.

(C) V_{oc} versus light intensity for the control devices and CB-PSCs.

(D) Mott-Schottky plot comparison of the control devices and CB-PSCs.

(E) EQE of EL of the devices while operating as LEDs. Inset: EL image of the devices under voltage bias.

(F) The ion E_a of perovskite films.

and perovskites. Furthermore, a comprehensive discussion about thermogravimetric analysis (Figure S35), SEM (Figures S36A and S36B), GIWAXS (Figures S36C and S36D), and AFM (Figures S36E and S36F) findings has been presented in Note S11, which are in good agreement with XRD results.

To clarify the underlying physical mechanisms of the covalent bonding strategy in enhancing the photovoltaic performance of CB-PSCs, we first investigated the trap density (N_t) of devices by using the space charge-limited current (SCLC) method. The electron-only device with structures of ITO/SnO_2/perovskite/[6,6]-phenyl-C61-butyric acid methyl ester (PCBM)/Au was fabricated, and the results are shown in Figure 4B. Trap-filled voltage (V_{TFL}) is related to trap density, according to the following equation:

$$V_{TFL} = \frac{qN_tL^2}{2\varepsilon\varepsilon_0} \qquad \text{(Equation 1)}$$

where ε is the dielectric constant of the perovskite, ε_0 is the vacuum permittivity, q is the elementary charge, and L is the thickness of the perovskite film. According to the curve of capacitance versus frequency (Figure S37), the dielectric constant can be calculated.[49] By employing the covalent bonding strategy, the V_{TFL} and N_t of the devices reduced from 0.94 V and 1.17 × 10^{16} cm^3 to 0.74 V and 8.01 × 10^{15} cm^3, respectively. In addition, the V_{oc} of the devices under different light intensities were recorded (Figure 4C). We found that the control device showed a slope of

Please cite this article in press as: Liu et al., Covalent bonding strategy to enable non-volatile organic cation perovskite for highly stable and efficient solar cells, Joule (2023), https://doi.org/10.1016/j.joule.2023.03.019

1.94 k_BT/q, whereas CB-PSCs exhibited a much smaller slope of 1.52 k_BT/q, where k_B is the Boltzmann constant and T is temperature. Generally, the slope of deviation from unity k_BT/q usually reflects trap-assisted non-radiative recombination in PSCs,[43] and the smaller slope of CB-PSCs indicates that there are fewer defects in perovskites. Furthermore, Mott-Schottky analyses of PSCs were conducted under a frequency of 10 kHz with bias voltages ranging from 0 to 1.3 V (Figure 4D). It is depicted that the built-in potential (V_{bi}) increased from 0.99 V for control devices to 1.05 V for CB-PSCs, which is consistent with the increased V_{oc} of CB-PSCs extracted from J-V curves. There is an accepted scientific principle that an efficient solar cell has to be an efficient light emitting diode (LED). Since CB-PSCs exhibit ultrahigh V_{oc} over 1.2 V, we therefore tested the solar cell device as an LED in the dark and under a voltage bias to estimate the recombination in devices (Figure 4E). We found that CB-PSCs showed an EL efficiency close to 11% under an injection current of 24.13 mA cm^{-2}, whereas the control device showed an EL efficiency of 6% under almost the same injection current. We then calculated the V_{oc} loss for the non-radiative recombination (ΔV_{oc}) according to the value of EQE_{EL}.[50] ΔV_{oc} of CB-PSCs is only 57 mV, which is one of the lowest reported ΔV_{oc} in PSCs to the best of our knowledge.[43,51]

Previous studies[13,14,16,17] have demonstrated that the loss of organic components from perovskite during the annealing period inevitably induces numerous vacancies (organic cation vacancies and halide vacancies). These defects not only accelerate the ion migration but also induce serious non-radiative recombination in PSCs.[13,18] Thus, the suppressed non-radiative recombination and lower trap density may be ascribed to the fact that the covalent bonding strategy effectively inhibits the loss of organic components. The well-suppressed non-radiative recombination by the covalent bonding strategy contributes to the ultrahigh efficiency and stability of CB-PSCs.

It is important to mention that the reduced hysteresis index (HI) and enhanced operational stability are partially related to ion migration induced by electric bias.[18,25,26,40] Moreover, numerous vacancies induced by the loss of MA^+, FA^+, and I^- can significantly accelerate ion migration by decreasing the energy barrier of migration.[18] In this context, Hui et al.[15] demonstrated that the presence of organic cation vacancies facilitates the migration of iodide ions due to the reduced steric hindrance. Therefore, to further verify the effect of the covalent bonding strategy on the immobilization of the organic cations, temperature-dependent electric conductivities were applied to measure the ion migration activation energy (ion E_a) of the perovskite films. The ion E_a plots depicted in Figures 4F and S38 demonstrated that the ion migration activation energy of perovskite films monotonously increased from 0.55 to 0.71 eV with the increased concentration of incorporated BD molecules. The increased ion E_a of the CB-perovskite film can be ascribed to the immobilization of organic components originating from the formation of covalent bonds with BD molecules, resulting in low-level densities of organic cation vacancies and iodide vacancies.[13,14,16] Moreover, the increased ion E_a of CB-perovskites is also consistent with the alleviated burn-in loss of CB-PSCs at the initial stage[39] and reduced hysteresis of CB-PSCs,[18] shown in Figures 3B, 3C, 3G, and 3H.

To further clarify the effect of the covalent bonding strategy on the stability of the devices, XPS and SEM were conducted to investigate the perovskite films before and after the aging period. As depicted in Figures 5B, 5D, 5F, 5H, and S39, the significant signals of F elements were detected only in CB-perovskite films, resulting from the introduction of BD molecules. In addition, after storing for 12 days with light illumination, for the Pb 4f XPS spectra of films (Figures 5A, 5C, 5E, and 5G), we

Please cite this article in press as: Liu et al., Covalent bonding strategy to enable non-volatile organic cation perovskite for highly stable and efficient solar cells, Joule (2023), https://doi.org/10.1016/j.joule.2023.03.019

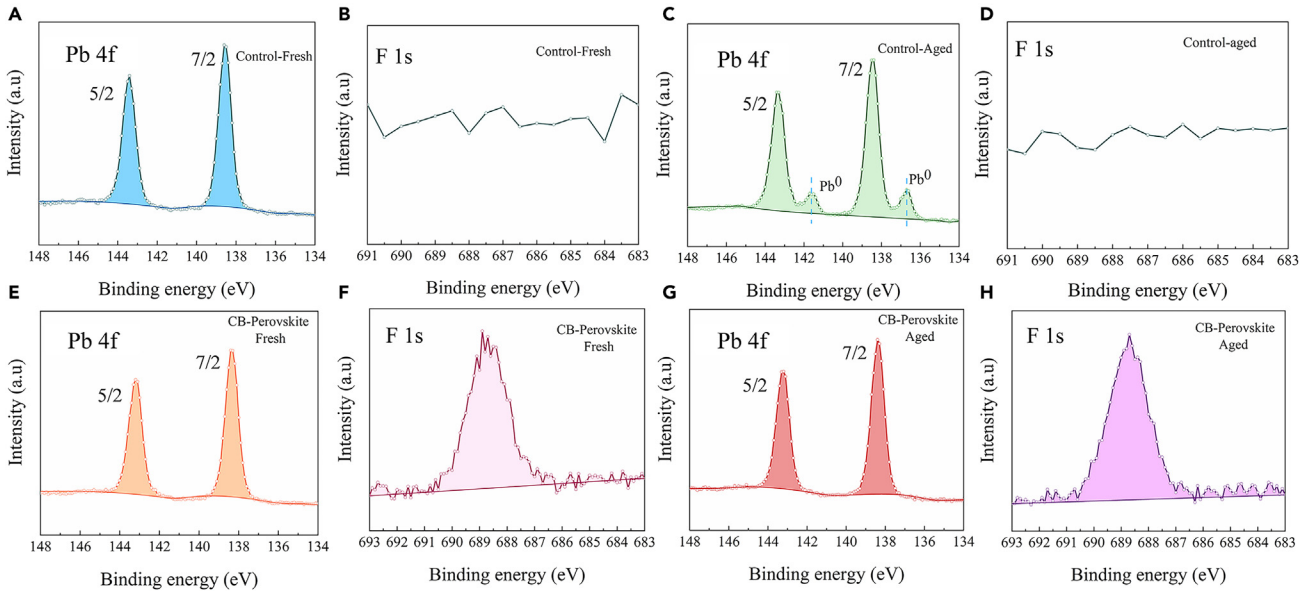

Figure 5. XPS spectra of perovskite films before and after the aging period

(A–D) XPS spectra of control films before and after the aging period: (A) and (C) deconvoluted XPS spectra for Pb 4f before and after the aging period; (B) and (D) deconvoluted XPS spectra for F 1s before and after the aging period.

(E–H) XPS spectra of CB-perovskite films before and after the aging period: (E) and (G) deconvoluted XPS spectra for Pb 4f before and after the aging period; (F) and (H) deconvoluted XPS spectra for F 1s before and after the aging period.

found that the control film showed clear signals of metallic Pb (Pb^0) peaks around 141.6 and 136.7 eV,[22] whereas the peak of metallic Pb disappeared in covalently bonded perovskite films with BD molecules. Importantly, metallic Pb as a primary deep defect state can deteriorate the performance and long-term stability of PSCs.[14,28,52] Some studies demonstrated that metallic Pb originates from the degradation of excessive PbI_2.[27,52] However, since the fabrication method of our PSCs is two-step sequential spin-coating method (Figure 1C), the perovskite film fabricated by this method usually contains some excessive PbI_2 at the surface.[43] As shown in Figures 4A and S36, even the CB-perovskite films still exhibited some excessive PbI_2 at the surface, but negligible metallic Pb appeared in CB-perovskite films and CB-PSCs exhibited excellent operational stability. This implies that in our work, metallic Pb may not be derived from excessive PbI_2. In addition, intensive research also have shown that halide and cation vacancies can easily induce the generation of unsaturated Pb that is considered the main factor for the generation of metallic Pb (Pb^0) under stimuli of light or heat.[14,19–21,23,24,53] The halide and cation vacancies can be triggered by the loss of organic components,[11,13,14,16,17,24] which contribute to ion migration by decreasing the E_a.[15,18] This is also in agreement with the increased E_a by the covalent bonding strategy (Figure 4F). Therefore, these results clearly demonstrate that the well-inhibited loss of organic components by the covalent bonding strategy contributes to less halide and cation vacancies, resulting in negligible metallic Pb in CB-perovskite films. Thus, the negligible metallic Pb in CB-perovskite films facilitates in suppressing the non-radiative recombination and ultimately elevating the photovoltaic performance of CB-PSCs and increasing the lifespan of devices.

In addition, it is reported that during the aging period, trace organic vapors such as MA, FA generated from the perovskite layer can accumulate underneath the gold (Au) electrode that ultimately trigger internal stress to form cracks on the Au

Please cite this article in press as: Liu et al., Covalent bonding strategy to enable non-volatile organic cation perovskite for highly stable and efficient solar cells, Joule (2023), https://doi.org/10.1016/j.joule.2023.03.019

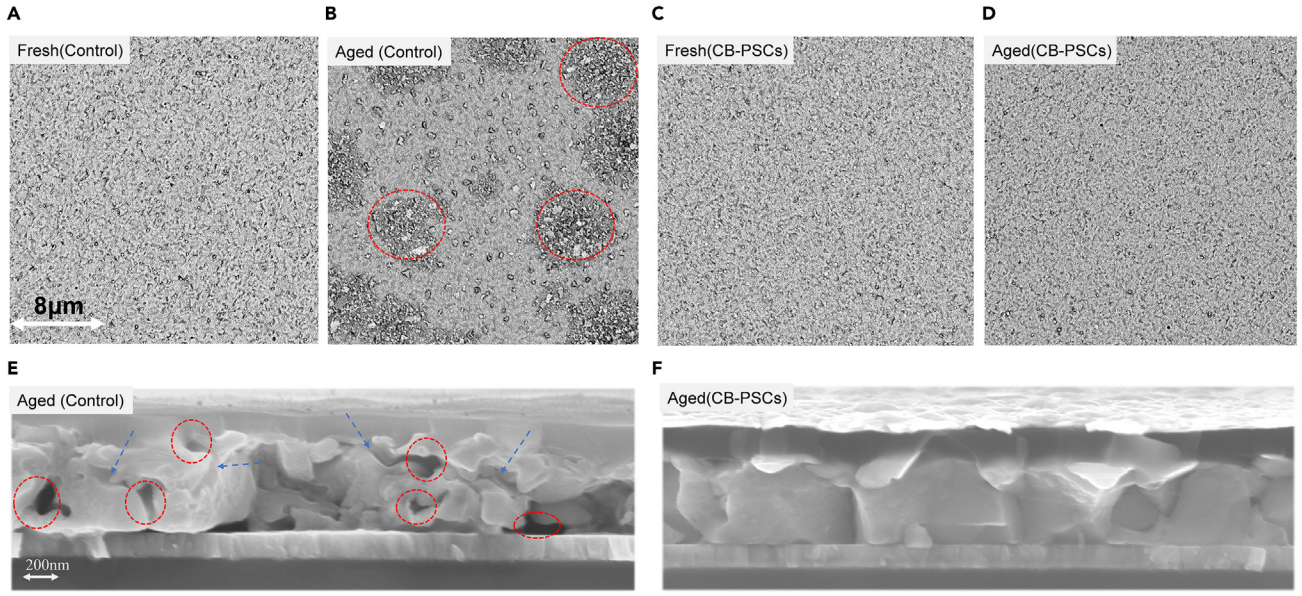

Figure 6. SEM images of PSCs before and after the aging period

(A–D) SEM (top view) of the devices' gold electrode.

(A) SEM of the fresh control device.

(B) SEM of the control device after aging.

(C) SEM of the fresh CB-PSC.

(D) SEM of the CB-PSC after aging (aging devices were put on a hot plate at 60°C for 414 h).

(E and F) Cross-sectional SEM images of the devices after aging. (E) Cross-sectional SEM image of the control device after aging; (F) cross-sectional SEM image of the CB-PSC after aging. (Devices were tracked at MPP for 1,120 h.).

surface.[12] Furthermore, Fan et al.[11] demonstrated that the loss of organic molecules during the aging period plays a critical role in inducing the release of I_2 vapor. The demeritorious I_2 vapors result in the further degradation of perovskites and induce the generation of more I_2 and metallic Pb leading to accelerated decomposition. Therefore, the morphology of the gold electrode of the devices before and after thermal aging has been investigated, and the results are shown in Figures 6A–6D. The SEM images of the control device clearly show the ruptured surface of the gold electrode after 414 h of aging at 60°C (Figure 6B, dashed circles). Interestingly, the CB-PSCs did not show significant deterioration or cracking on the surface of the gold electrode (Figure 6D), and it is similar to that of the fresh device (Figure 6C), which is attributed to the development of covalent linkage with BD molecules. In addition, XPS analysis has been employed to further prove the efficacy of our strategy to protect perovskites under stimuli of heat, as shown in Figures S40–S42. These aged films were placed on the 85°C hotplate for 48 h in a nitrogen glovebox. After aging, compared with the CB-perovskite, the C 1s and N 1s intensities of the control films decreased obviously, which demonstrated that BD molecules effectively immobilized organic cations during the aging period. Moreover, the XPS analysis of the Pb element illustrated that after aging, a clear signal of metallic Pb appeared in the control film, however, it was not observed in aged CB-perovskite. This is also consistent with Figure 5, as mentioned above, which is attributed to the loss of organic components. Thus, CB-PSCs exhibit excellent thermal stability (Figure 3I). Moreover, the excellent operational stability of CB-PSCs can also be confirmed by cross-sectional SEM images of devices after 1,120 h MPPT. As depicted in Figure 6E, after MPPT, the control device showed irreversible morphological degradation features with obvious voids (indicated by dashed circles) and fracture crystals. More importantly, it seems that some channels

Please cite this article in press as: Liu et al., Covalent bonding strategy to enable non-volatile organic cation perovskite for highly stable and efficient solar cells, Joule (2023), https://doi.org/10.1016/j.joule.2023.03.019

(indicated by blue arrows) appeared around these voids, which may stem from the escape of organic components. In contrast, after 1,120 h MPPT, CB-PSC exhibited compact and homogeneous crystal grains without any visible voids (Figure 6F). These results further confirm that the degradation of perovskite could be effectively alleviated through the covalent bonding strategy.

Conclusions

In summary, a novel covalent bonding strategy incorporating BD molecules to bind organic cations of perovskite has been proposed to achieve highly efficient and ultra-stable PSCs. The resulting device yielded PCEs of 23.95% (1.57 eV) and 24.36% (1.53 eV), showing less hysteresis and excellent long-term operational stability while retaining 98.6% of the initial efficiency after 1,000 h MPPT and continuous illumination. By contrast, the control devices decayed to 65% of the initial PCE only after 200 h of the aging test. The CB-PSCs also demonstrated tremendous thermal stability while retaining 97.6% of the initial efficiency even at 60°C after ~590 h. The efficacy of this covalent bonding strategy has been further elucidated by several characterization methods along with density functional theory (DFT) simulation, and it has been deduced that it can simultaneously enable multiple outstanding functionalities of perovskite films including reduced defects, inhibition of ion migration, negligible metallic Pb, and eliminated trace organic vapors under stimuli of heat and light, contributing to the improved photovoltaic performance and stability of devices. This work suggests a novel and effective strategy to confine the loss of organic components from perovskites to realize highly efficient and ultra-stable PSCs. Moreover, this strategy possesses great potential in other perovskite-based optoelectronic devices.

EXPERIMENTAL PROCEDURES

Resource availability

Lead contact

Further information and requests for resources should be directed to and will be fulfilled by the lead contact, Yiqiang Zhan (yqzhan@fudan.edu.cn).

Materials Availability

This study did not generate new unique reagents.

Data and code availability

This study did not generate any datasets.

Materials

Dimethylformamide (DMF), dimethyl sulfoxide (DMSO), chlorobenzene, isopropyl alcohol (IPA), lithium bis (trifluoromethanesulfonyl)imide salt (Li-TFSI), and 4-tert-butylpyridine (tBP) were purchased from Sigma-Aldrich. SnO_2 colloid precursor (tin (iv) oxide, 15% in H_2O colloidal dispersion) was purchased from Alfa Aesar. DMF 2, 2′, 7, 7′ Tetrakis (N, N-di-p-methoxyphenylamino)-9, 9′-spirobifluorene (spiro-OMeTAD), PTAA (Mn 6,000–15,000) and Tris(2-(1H-pyrazol-1-yl)-4-tert-butylpyridine) cobalt (III)Tris(bis(trifluoromethylsulfonyl)imide) salt (Co (III) TFSI), PEAI were purchased from Xi'an Polymer Light Technology Corp. PbI_2 was purchased from TCI. Tetrakis(pentafluorophenyl)borate (TPFB) (≥98.0%) was obtained from TCI Inc. FAI, methylammonium bromide (MABr), methylammonium chloride (MACl) were purchased from Advanced Election Technology Co., Ltd. The 3,3′-((perfluoropropane-2,2-diyl) *bis*(4,1-phenylene)) *bis*(3-(trifluoromethyl)-3*H*-diazirine) (BD molecule) was provided by XlynX Materials.

Please cite this article in press as: Liu et al., Covalent bonding strategy to enable non-volatile organic cation perovskite for highly stable and efficient solar cells, Joule (2023), https://doi.org/10.1016/j.joule.2023.03.019

Device fabrication

The indium tin oxide (ITO) substrates were sequentially washed with ethyl alcohol, acetone, DI water followed by N_2 blow dry. The SnO_2 spin-coating solution was prepared by dissolving 2.67% of SnO_2 nanoparticles into the DI water under constant stirring for 5 min at room temperature. Then SnO_2 aqueous solution was spin coated at 3,000 rpm for 30 s and then annealed in vacuum at 80°C for 30 min. It was then treated with UV Ozone for 15 min. The perovskite precursor was prepared from 1.3 M PbI_2 in DMF:DMSO = 9:1 solution and mixed organic salts (FAI:MABr:MACl = 60 mg:6 mg) in 1 mL IPA, respectively. The 1.5 M thicker FA-based perovskite was prepared from 1.5 M PbI_2 in DMF:DMSO = 9:1 solution and mixed organic salts (FAI:MAI:MACl = 90 mg:6.4 mg:9 mg) in 1 mL IPA, respectively. Further, 6 mg PEAI was dissolved in 1 mL IPA and stirred at room temperature for 5 h. The BD molecules was first dissolved in DMF and then added into the PbI_2 solution with an optimized molar ratio. A two-step spin-coating method was adopted to deposit perovskite layer. Filtration is required before using the PbI_2 precursor. The PbI_2 precursors with different molar ratios of BD molecules were spin coated at 1,500 rpm for 30 s onto the SnO_2 and then annealed at 70°C for 1 min. The PbI_2 films were then allowed to cool down. Further, the organic salts solution was spin coated onto PbI_2 at 2,200 rpm for 3 s, 1,300 rpm for 15 s and then 1,700 rpm for 12 s, followed by thermal annealing at 150°C for 15 min in ambient atmospheric conditions (33%–38% humidity). The value of humidity is important for the performance of fabricated PSCs. The annealing temperature is enough to assist BD molecules to react with perovskite. Then, PEAI solution was spin coated at 4,500 rpm for 30 s onto perovskite to passivate the interface defects. Afterward, the hole transporting layer (HTL) was coated on perovskite film at 3,000 rpm for 30 s. The HTL solution consists of 72.3 mg of spiro-OMeTAD, 29 μL of tBP, 18 μL of Co (III) TFSI solution (300 mg mL^{-1} in acetonitrile), 25 μL of Li-TFSI solution (520 mg mL^{-1} in acetonitrile), and 1 mL of chlorobenzene. Spiro-OMeTAD was replaced by ploy[bis(4-phenyl)(2,4,6-triMethyphenyl) aMine] (PTAA) for thermal stability. PTAA solution (15 mg/mL; in CB with 5% TPFB) was spun onto the perovskite film at 3,000 rpm for 30 s. The HTL solution preparation and deposition were performed inside a nitrogen glovebox. Finally, the Au back electrode (85 nm) was deposited by thermal evaporation.

Material characterization

The XRD measurements were carried out using X-ray diffractometer (D8 Advance) with a monochromatic Cu-Kα (λ = 1.5405 Å) X-ray source. SEM images of perovskite films were taken by Hitachi S-4800 and ZEISS SIGMA HD. FTIR spectra were recorded by IR spectrometer instrument (BRUKER, VERTEX 70). NMR spectra were recorded at ambient temperature using a Bruker AVANCE 300 (300.27 MHz for ^{1}H, 282.54 MHz for ^{19}F). Chemical shifts were reported in ppm and were calibrated to the central peak of residual NMR solvent (central peak of chloroform-d: ^{1}H NMR δ = 7.26 ppm). Data are reported as follows: chemical shift (multiplicity [s, singlet; d, doublet; t, triplet; q, quartet; sept, septet; m, multiplet; br, broad singlet], coupling constant in Hz, integration). BD molecule was dissolved in 15 mM solution of isopropylamine (model compound for MA^{+}) in a heavy wall pressure vessel and the molecule was activated at 110°C for 30 min. After evaporation of residual isopropylamine, the crude material was purified by silica gel chromatography. The final product spectra were compared with previously reported spectroscopic data. Thermogravimetric analysis (TGA) measurements were performed using a Pyris 1 thermal analysis system, heating at a rate of 5°C min from 300 to 550 K under a constant N_2 gas flow. Synchrotron-based GIWAXS measurements were performed at the BL14B1 beamline of the Shanghai Synchrotron Radiation Facility (SSRF) using X-rays with a wavelength of 1.2398 Å. Two-dimensional (2D) GIWAXS patterns were acquired by a Pilatas2M detector mounted vertically at a distance of ~251 mm from the sample with a

Please cite this article in press as: Liu et al., Covalent bonding strategy to enable non-volatile organic cation perovskite for highly stable and efficient solar cells, Joule (2023), https://doi.org/10.1016/j.joule.2023.03.019

grazing incidence angle of 0.4°. XPS data were measured in an ultrahigh vacuum surface analysis system equipped with SCIENTA R3000 spectrometer with a base pressure of 10^{-10} mbar and with monochromatic Al Kα 1,486.6 eV source. All of aged samples were stored for 12 days with light illumination in N_2 glovebox, then XPS was employed to explore the elemental changes on the surface of perovskite. All the thermal aged perovskite film were put on 85° hotplate for 48 h. All spectra ware calibrated by referring to Fermi level edge and Au 4f7/2 position of the Ar^+ ion sputter-cleaned Au film.

Devices characterization

The J-V curves of the PSCs were measured using a Keithley 2602B source in the N_2 filled glove box at room temperature under AM 1.5 G condition at an intensity of 100 mW/cm^2, calibrated by a standard Si solar cell (PVM937, Newport) (Data S1.). The standard Si is calibrated every month. A 450-watt xenon lamp (Oriel solar simulator, 94023A) was used as a light source. The active area of PSCs is 0.105 cm^2 defined by the cross of patterned Au and ITO electrode, and further calibrated by the microscope. The aperture area is 0.0865 cm^2. The J-V curves were obtained both at forward scan (from −0.2 to 1.22 V, step 0.02 V) and reverse scan (from 1.22 to −0.2 V, step 0.02 V) without any pre-conditioning before the test. EQE data were acquired by an EQE system (Enli Tech, Taiwan) using 100 Hz chopped monochromatic light (300–900 nm). Thermal stability test was performed under N_2 glove box. Samples were annealed at 60°C and 85°C using hotplate. Similar to previously reported works,[5,43] to exclude the influence of spiro-OMeTAD, we replaced it with PTAA. Operational stability was tested using white LED at 100 mW/cm^2 without UV filter. Samples were under illumination in an N_2 environment at 36°C ± 3°C without any encapsulation. Maximum power point (MPP) dynamic tracking test adopts disturbance observation tracking. We first set the MPPT test duration t, and then set the number of IV scans in the test (for example, if the test duration is 1,000 h and the number of IV scans are 40 times, IV scans will be performed every 25 h in the test). For each IV scan, Vmax1 of the current scan was captured as the disturbance base, and 25 step scans were performed at plus/minus 50 mV. Vmax2 within the recording interval was captured and multiplied by the current at that time to obtain a MPP, and a MPP was recorded according to the MPPT scanning interval. In this way, V_{max} has been updated after each scan and the next perturbation scan is performed in the vicinity of V_{max}. For the device operating as an LED, the device was mounted in an integrating sphere and the power output was measured for calculation of the EQE (Enlitech). Mott-Schottky curves with capacitance-voltage measurements were performed by a ZAHNER PP211 electrochemical workstation at 10 kHz with bias voltages ranging from 1.3 to 0 V and an AC voltage of 20 mV was used to test the corresponding capacitance at shifty bias voltage. The built-in potential (Vbi) in the perovskite layers can be estimated by following depletion approximation equation (Mott-Schottky).[52] Activation energy measurement of ion migration was carried out by measuring the temperature-dependent electric conductivity of Au/perovskite/Au structure under an electric field of 0.35 Vμm^{-1}. The activation energy E_a can be extracted by fitting the raw data points to the Arrhenius equation.[54]

DFT computational details

All the first-principles calculations were performed based on DFT as implemented by the Vienna Ab-initio Simulation Package (VASP) code.[55] The Perdew-Burke-Ernzerhof (PBE)[55] exchange correlation functional form of the generalized gradient approximation (GGA) was used with a 400 eV cutoff energy for the plane wave basis. All the surface structures in this study were constructed based on 2 × 2 × 3 supercell (156 atoms) of the relaxed 12-atom primitive cell of $FAPbI_3$ and the surface is (001). All the relaxation and self-consistent calculations of surface structures were carried

out by using a 3 × 3 × 1 Monkhorst-Pack k-point mesh.[56] The atomic layers of the formula unit at the bottom were fixed when the relaxation of surface structures was performed. The convergence criteria of the surface structure relaxation is 0.05 eV/Å. In order to remove the interaction between the mirror images of slab models along [001] direction, a vacuum layer lager than 15 Å was used to isolate the slab models.

SUPPLEMENTAL INFORMATION

Supplemental information can be found online at https://doi.org/10.1016/j.joule.2023.03.019.

ACKNOWLEDGMENTS

This work was supported by the National Natural Science Foundation of China (no. 62274040). All the authors sincerely thank XlynX Materials for providing us the outstanding BD molecules (BondLynx-Gen-I). All the authors sincerely thank Dr. Liting Yang and Prof. Renchao Che for supporting the HAADF and EDS tests.

AUTHOR CONTRIBUTIONS

Y.Z. conceived the idea. Y.Z., A.Y., and J.E.W. directed and supervised the project. K.L. initialized this project and fabricated the devices. S.F.M. and J.E.W. provided BD molecules. S.F.M. carried out the NMR experiment. F.L. took part in the device fabrication and characterization. Z.C. and S.C. performed DFT simulation. Y. Yuan., C.N., and X.P. performed ion migration tests. L.S. and J.C. did the FTIR measurement. W.Y. and S.Z. performed TGA measurement. K.L. carried out stability tests. Y.P. did the XRD test. K.L. wrote the first draft of the paper. S.R., Y.Z., and A.Y. modified the paper. All authors contributed to discussions and finalizing the manuscript.

DECLARATION OF INTERESTS

The authors declare no competing interests.

Received: April 12, 2022
Revised: October 20, 2022
Accepted: March 28, 2023
Published: April 20, 2023

REFERENCES

1. Yoo, J.J., Seo, G., Chua, M.R., Park, T.G., Lu, Y., Rotermund, F., Kim, Y.-K., Moon, C.S., Jeon, N.J., Correa-Baena, J.-P., et al. (2021). Efficient perovskite solar cells via improved carrier management. Nature *590*, 587–593. https://doi.org/10.1038/s41586-021-03285-w.

2. Jeong, J., Kim, M., Seo, J., Lu, H.Z., Ahlawat, P., Mishra, A., Yang, Y.G., Hope, M.A., Eickemeyer, F.T., Kim, M., et al. (2021). Pseudo-halide anion engineering for alpha-FAPbI(3) perovskite solar cells. Nature *592*, 381–385. https://doi.org/10.1038/s41586-021-03406-5.

3. Min, H., Lee, D.Y., Kim, J., Kim, G., Lee, K.S., Kim, J., Paik, M.J., Kim, Y.K., Kim, K.S., Kim, M.G., et al. (2021). Perovskite solar cells with atomically coherent interlayers on SnO2 electrodes. Nature *598*, 444–450. https://doi.org/10.1038/s41586-021-03964-8.

4. Jiang, Q., Tong, J., Xian, Y., Kerner, R.A., Dunfield, S.P., Xiao, C., Scheidt, R.A., Kuciauskas, D., Wang, X., Hautzinger, M.P., et al. (2022). Surface reaction for efficient and stable inverted perovskite solar cells. Nature *611*, 278–283. https://doi.org/10.1038/s41586-022-05268-x.

5. Zhao, Y., Ma, F., Qu, Z., Yu, S., Shen, T., Deng, H.-X., Chu, X., Peng, X., Yuan, Y., Zhang, X., and You, J. (2022). Inactive (PbI2)2RbCl stabilizes perovskite films for efficient solar cells. Science *377*, 531–534. https://doi.org/10.1126/science.abp8873.

6. Boyd, C.C., Cheacharoen, R., Leijtens, T., and McGehee, M.D. (2019). Understanding degradation mechanisms and improving stability of perovskite photovoltaics. Chem. Rev. *119*, 3418–3451. https://doi.org/10.1021/acs.chemrev.8b00336.

7. Bryant, D., Aristidou, N., Pont, S., Sanchez-Molina, I., Chotchunangatchaval, T., Wheeler, S., Durrant, J.R., and Haque, S.A. (2016). Light and oxygen induced degradation limits the operational stability of methylammonium lead triiodide perovskite solar cells. Energy Environ. Sci. *9*, 1655–1660. https://doi.org/10.1039/C6EE00409A.

8. Juarez-Perez, E.J., Hawash, Z., Raga, S.R., Ono, L.K., and Qi, Y. (2016). Thermal degradation of CH3NH3PbI3 perovskite into NH3 and CH3I gases observed by coupled thermogravimetry–mass spectrometry analysis. Energy Environ. Sci. *9*, 3406–3410. https://doi.org/10.1039/C6EE02016J.

9. Mei, A., Sheng, Y., Ming, Y., Hu, Y., Rong, Y., Zhang, W., Luo, S., Na, G., Tian, C., Hou, X., et al. (2020). Stabilizing perovskite Solar Cells to IEC61215:2016 Standards with over 9,000-h Operational Tracking. Joule *4*, 2646–2660. https://doi.org/10.1016/j.joule.2020.09.010.

10. Shi, L., Bucknall, M.P., Young, T.L., Zhang, M., Hu, L., Bing, J., Lee, D.S., Kim, J., Wu, T.,

Takamure, N., et al. (2020). Gas chromatography-mass spectrometry analyses of encapsulated stable perovskite solar cells. Science *368*, eaba2412. https://doi.org/10.1126/science.aba2412.

11. Fu, F., Pisoni, S., Jeangros, Q., Sastre-Pellicer, J., Kawecki, M., Paracchino, A., Moser, T., Werner, J., Andres, C., Duchêne, L., et al. (2019). I2 vapor-induced degradation of formamidinium lead iodide based perovskite solar cells under heat–light soaking conditions. Energy Environ. Sci. *12*, 3074–3088. https://doi.org/10.1039/C9EE02043H.

12. Zhao, Y., Heumueller, T., Zhang, J., Luo, J., Kasian, O., Langner, S., Kupfer, C., Liu, B., Zhong, Y., Elia, J., et al. (2022). A bilayer conducting polymer structure for planar perovskite solar cells with over 1,400 hours operational stability at elevated temperatures. Nat. Energy *7*, 144–152. https://doi.org/10.1038/s41560-021-00953-z.

13. Zheng, X.P., Chen, B., Dai, J., Fang, Y.J., Bai, Y., Lin, Y.Z., Wei, H.T., Zeng, X.C., and Huang, J.S. (2017). Defect passivation in hybrid perovskite solar cells using quaternary ammonium halide anions and cations. Nat. Energy *2*, 17102. https://doi.org/10.1038/nenergy.2017.102.

14. Du, Y., Wu, J., Zhang, X., Zhu, Q., Zhang, M., Liu, X., Zou, Y., Wang, S., and Sun, W. (2021). Surface passivation using pyridinium iodide for highly efficient planar perovskite solar cells. J. Energy Chem. *52*, 84–91. https://doi.org/10.1016/j.jechem.2020.04.049.

15. Yu, H., Lu, H., Xie, F., Zhou, S., and Zhao, N. (2016). Native defect-induced hysteresis behavior in organolead iodide perovskite solar cells. Adv. Funct. Mater. *26*, 1411–1419. https://doi.org/10.1002/adfm.201504997.

16. Chen, S., Wu, C., Han, B., Liu, Z., Mi, Z., Hao, W., Zhao, J., Wang, X., Zhang, Q., Liu, K., et al. (2021). Atomic-scale imaging of CH3NH3PbI3 structure and its decomposition pathway. Nat. Commun. *12*, 5516. https://doi.org/10.1038/s41467-021-25832-9.

17. Yang, X., Ni, Y., Zhang, Y., Wang, Y., Yang, W., Luo, D., Tu, Y., Gong, Q., Yu, H., and Zhu, R. (2021). Multiple-defect management for efficient perovskite photovoltaics. ACS Energy Lett. *6*, 2404–2412. https://doi.org/10.1021/acsenergylett.1c01039.

18. Yuan, Y., and Huang, J. (2016). Ion migration in organometal trihalide perovskite and its impact on photovoltaic efficiency and stability. Acc. Chem. Res. *49*, 286–293. https://doi.org/10.1021/acs.accounts.5b00420.

19. Sun, C., Wei, J., Zhao, J., Jiang, Y., Wang, Y., Hu, H., Wang, X., Zhang, Y., and Yuan, M. (2021). Hard and soft Lewis-base behavior for efficient and stable CsPbBr3 perovskite light-emitting diodes. Nanophotonics *10*, 2157–2166. https://doi.org/10.1515/nanoph-2021-0003.

20. Chen, J., Yang, Y., Dong, H., Li, J., Zhu, X., Xu, J., Pan, F., Yuan, F., Dai, J., Jiao, B., et al. (2022). Highly efficient and stable perovskite solar cells enabled by low-dimensional perovskitoids. Sci. Adv. *8*, eabk2722. https://doi.org/10.1126/sciadv.abk2722.

21. Zhang, W., Pathak, S., Sakai, N., Stergiopoulos, T., Nayak, P.K., Noel, N.K., Haghighirad, A.A., Burlakov, V.M., deQuilettes, D.W., Sadhanala, A., et al. (2015). Enhanced optoelectronic quality of perovskite thin films with hypophosphorous acid for planar heterojunction solar cells. Nat. Commun. *6*, 10030. https://doi.org/10.1038/ncomms10030.

22. Zhang, H., Chen, Z., Qin, M., Ren, Z., Liu, K., Huang, J., Shen, D., Wu, Z., Zhang, Y., Hao, J., et al. (2021). Multifunctional crosslinking-enabled strain-regulating crystallization for stable, efficient alpha-FAPbI3 -Based perovskite solar cells. Adv. Mater. *33*, e2008487. https://doi.org/10.1002/adma.202008487.

23. Chen, H., Liu, T., Zhou, P., Li, S., Ren, J., He, H., Wang, J., Wang, N., and Guo, S. (2020). Efficient bifacial passivation with crosslinked thioctic acid for high-performance methylammonium lead iodide perovskite solar cells. Adv. Mater. *32*, e1905661. https://doi.org/10.1002/adma.201905661.

24. Tang, X., Brandl, M., May, B., Levchuk, I., Hou, Y., Richter, M., Chen, H., Chen, S., Kahmann, S., Osvet, A., et al. (2016). Photoinduced degradation of methylammonium lead triiodide perovskite semiconductors. J. Mater. Chem. A *4*, 15896–15903. https://doi.org/10.1039/C6TA06497C.

25. Lin, D.X., Shi, T.T., Xie, H.P., Wan, F., Ren, X.X., Liu, K., Zhao, Y., Ke, L.L., Lin, Y., Gao, Y.L., et al. (2021). Ion migration accelerated reaction between oxygen and metal halide perovskites in light and its suppression by cesium incorporation. Adv. Energy Mater. *11*, 2002552. https://doi.org/10.1002/aenm.202002552.

26. Tan, S., Yavuz, I., De Marco, N., Huang, T., Lee, S.J., Choi, C.S., Wang, M., Nuryyeva, S., Wang, R., Zhao, Y., et al. (2020). Steric impediment of ion migration contributes to improved operational stability of perovskite solar cells. Adv. Mater. *32*, e1906995. https://doi.org/10.1002/adma.201906995.

27. Tumen-Ulzii, G., Qin, C., Klotz, D., Leyden, M.R., Wang, P., Auffray, M., Fujihara, T., Matsushima, T., Lee, J.W., Lee, S.J., et al. (2020). Detrimental effect of unreacted PbI2 on the long-term stability of perovskite solar cells. Adv. Mater. *32*, e1905035. https://doi.org/10.1002/adma.201905035.

28. Wang, L., Zhou, H., Hu, J., Huang, B., Sun, M., Dong, B., Zheng, G., Huang, Y., Chen, Y., Li, L., et al. (2019). A Eu3+-Eu2+ ion redox shuttle imparts operational durability to Pb-I perovskite solar cells. Science *363*, 265–270. https://doi.org/10.1126/science.aau5701.

29. Zhang, H., Hou, M., Xia, Y., Wei, Q., Wang, Z., Cheng, Y., Chen, Y., and Huang, W. (2018). Synergistic effect of anions and cations in additives for highly efficient and stable perovskite solar cells. J. Mater. Chem. A *6*, 9264–9270. https://doi.org/10.1039/C8TA00308D.

30. Xie, H., Wang, Z., Chen, Z., Pereyra, C., Pols, M., Gałkowski, K., Anaya, M., Fu, S., Jia, X., Tang, P., et al. (2021). Decoupling the effects of defects on efficiency and stability through phosphonates in stable halide perovskite solar cells. Joule *5*, 1246–1266. https://doi.org/10.1016/j.joule.2021.04.003.

31. Li, X., Zhang, W., Wang, Y.C., Zhang, W., Wang, H.Q., and Fang, J. (2018). In-situ cross-linking strategy for efficient and operationally stable methylammoniun lead iodide solar cells. Nat. Commun. *9*, 3806. https://doi.org/10.1038/s41467-018-06204-2.

32. Yang, S., Chen, S., Mosconi, E., Fang, Y., Xiao, X., Wang, C., Zhou, Y., Yu, Z., Zhao, J., Gao, Y., et al. (2019). Stabilizing halide perovskite surfaces for solar cell operation with wide-bandgap lead oxysalts. Science *365*, 473–478. https://doi.org/10.1126/science.aax3294.

33. Lepage, M.L., Simhadri, C., Liu, C., Takaffoli, M., Bi, L., Crawford, B., Milani, A.S., and Wulff, J.E. (2019). A broadly applicable cross-linker for aliphatic polymers containing C-H bonds. Science *366*, 875–878. https://doi.org/10.1126/science.aay6230.

34. Zhao, X., Bi, L., Khatir, B., Serles, P., Filleter, T., Wulff, J.E., and Golovin, K. (2022). Crosslinking inert liquidlike polydimethylsiloxane brushes using bis-diazirine chemical insertion for enhanced mechanical durability. Chem. Eng. J. *442*, 136017. https://doi.org/10.1016/j.cej.2022.136017.

35. Musolino, S.F., Pei, Z., Bi, L., DiLabio, G.A., and Wulff, J.E. (2021). Structure-function relationships in aryl diazirines reveal optimal design features to maximize C-H insertion. Chem. Sci. *12*, 12138–12148. https://doi.org/10.1039/d1sc03631a.

36. Deutsch, A., Glas, H., Hoffmann-Röder, A., and Deutsch, C. (2014). Synthesis of functionalized alpha-trifluoroethyl amine scaffolds via Grignard addition to N-aryl hemiaminal ethers. RSC Adv. *4*, 9288–9291. https://doi.org/10.1039/C3RA47708H.

37. Cao, Q., Li, Y., Zhang, H., Yang, J., Han, J., Xu, T., Wang, S., Wang, Z., Gao, B., Zhao, J., et al. (2021). Efficient and stable inverted perovskite solar cells with very high fill factors via incorporation of star-shaped polymer. Sci. Adv. *7*, eabg0633. https://doi.org/10.1126/sciadv.abg0633.

38. Li, N., Tao, S., Chen, Y., Niu, X., Onwudinanti, C.K., Hu, C., Qiu, Z., Xu, Z., Zheng, G., Wang, L., et al. (2019). Cation and anion immobilization through chemical bonding enhancement with fluorides for stable halide perovskite solar cells. Nat. Energy *4*, 408–415. https://doi.org/10.1038/s41560-019-0382-6.

39. Domanski, K., Roose, B., Matsui, T., Saliba, M., Turren-Cruz, S.-H., Correa-Baena, J.-P., Carmona, C.R., Richardson, G., Foster, J.M., De Angelis, F., et al. (2017). Migration of cations induces reversible performance losses over day/night cycling in perovskite solar cells. Energy Environ. Sci. *10*, 604–613. https://doi.org/10.1039/C6EE03352K.

40. van Reenen, S., Kemerink, M., and Snaith, H.J. (2015). Modeling anomalous hysteresis in perovskite solar cells. J. Phys. Chem. Lett. *6*, 3808–3814. https://doi.org/10.1021/acs.jpclett.5b01645.

41. Khenkin, M.V., Katz, E.A., Abate, A., Bardizza, G., Berry, J.J., Brabec, C., Brunetti, F., Bulović, V., Burlingame, Q., Di Carlo, A., et al. (2020). Consensus statement for stability assessment and reporting for perovskite photovoltaics based on ISOS procedures. Nat. Energy *5*, 35–49. https://doi.org/10.1038/s41560-019-0529-5.

42. Christians, J.A., Schulz, P., Tinkham, J.S., Schloemer, T.H., Harvey, S.P., Tremolet de Villers, B.J., Sellinger, A., Berry, J.J., and Luther, J.M. (2018). Tailored interfaces of unencapsulated perovskite solar cells for >1,000 hour operational stability. Nat. Energy *3*, 68–74. https://doi.org/10.1038/s41560-017-0067-y.

43. Jiang, Q., Zhao, Y., Zhang, X., Yang, X., Chen, Y., Chu, Z., Ye, Q., Li, X., Yin, Z., and You, J. (2019). Surface passivation of perovskite film for efficient solar cells. Nat. Photonics *13*, 460–466. https://doi.org/10.1038/s41566-019-0398-2.

44. Xiong, Z., Chen, X., Zhang, B., Odunmbaku, G.O., Ou, Z., Guo, B., Yang, K., Kan, Z., Lu, S., Chen, S., et al. (2022). Simultaneous interfacial modification and crystallization control by biguanide hydrochloride for stable perovskite solar cells with PCE of 24.4. Adv. Mater. *34*, e2106118. https://doi.org/10.1002/adma.202106118.

45. Huang, H., Cui, P., Chen, Y., Yan, L., Yue, X., Qu, S., Wang, X., Du, S., Liu, B., Zhang, Q., et al. (2022). 24.8%-efficient planar perovskite solar cells via ligand-engineered TiO2 deposition. Joule *6*, 2186–2202. https://doi.org/10.1016/j.joule.2022.07.004.

46. Gong, C., Zhang, C., Zhuang, Q., Li, H., Yang, H., Chen, J., and Zang, Z. (2022). Stabilizing buried interface via synergistic effect of fluorine and sulfonyl functional groups toward efficient and stable perovskite solar cells. Nanomicro Lett. *15*, 17. https://doi.org/10.1007/s40820-022-00992-5.

47. Ge, Y.S., Ye, F.H., Xiao, M., Wang, H.B., Wang, C., Liang, J.W., Hu, X.Z., Guan, H.L., Cui, H.S., Ke, W.J., et al. (2022). Internal encapsulation for lead halide perovskite films for efficient and very stable solar cells. Adv. Energy Mater. *12*, 2200361. https://doi.org/10.1002/aenm.202200361.

48. Liu, X., Zheng, B., Shi, L., Zhou, S., Xu, J., Liu, Z., Yun, J.S., Choi, E., Zhang, M., Lv, Y., et al. (2023). Perovskite solar cells based on spiro-OMeTAD stabilized with an alkylthiol additive. Nat. Photonics *17*, 96–105. https://doi.org/10.1038/s41566-022-01111-x.

49. Kang, D.-H., Kim, S.-Y., Lee, J.-W., and Park, N.-G. (2021). Efficient surface passivation of perovskite films by a post-treatment method with a minimal dose. J. Mater. Chem. A *9*, 3441–3450. https://doi.org/10.1039/D0TA10581C.

50. Rau, U. (2007). Reciprocity relation between photovoltaic quantum efficiency and electroluminescent emission of solar cells. Phys. Rev. B *76*, 085303. https://doi.org/10.1103/PhysRevB.76.085303.

51. Xi, J.C., Wu, Y.Y., Chen, W.J., Li, Q.L., Li, J.J., Shen, Y.X., Chen, H.Y., Xu, G.Y., Yang, H.Y., Chen, Z.Y., et al. (2022). Cross-linkable molecule in spatial dimension boosting water-stable and high-efficiency perovskite solar cells. Nano Energy *93*, 106846. https://doi.org/10.1016/j.nanoen.2021.106846.

52. Liang, J., Hu, X., Wang, C., Liang, C., Chen, C., Xiao, M., Li, J., Tao, C., Xing, G., Yu, R., et al. (2022). Origins and influences of metallic lead in perovskite solar cells. Joule *6*, 816–833. https://doi.org/10.1016/j.joule.2022.03.005.

53. Han, T.H., Zhao, Y., Yoon, J., Woo, J.Y., Cho, E.H., Kim, W.D., Lee, C., Lee, J.W., Choi, J.M., Han, J., et al. (2022). Spontaneous hybrid cross-linked network induced by multifunctional copolymer toward mechanically resilient perovskite solar cells. Adv. Funct. Mater. *32*, 2207142. https://doi.org/10.1002/adfm.202207142.

54. Yuan, Y.B., Chae, J., Shao, Y.C., Wang, Q., Xiao, Z.G., Centrone, A., and Huang, J.S. (2015). Photovoltaic switching mechanism in lateral structure hybrid perovskite solar cells. Adv. Energy Mater. *5*, 1500615. https://doi.org/10.1002/aenm.201500615.

55. Kresse, G., and Furthmüller, J. (1996). Efficient iterative schemes for ab initio total-energy calculations using a plane-wave basis set. Phys. Rev. B Condens. Matter *54*, 11169–11186. https://doi.org/10.1103/physrevb.54.11169.

56. Monkhorst, H.J., and Pack, J.D. (1976). Special points for Brillouin-zone integrations. Phys. Rev. B *13*, 5188–5192. https://doi.org/DOI. https://doi.org/10.1103/PhysRevB.13.5188.